Crystallized $InBiS_3$ thin films with enhanced optoelectronic properties

N. Ali[1, 2, **], Arshad Hussain[1,3], R. Ahmed[1, *], M. Firdaus Bin Omar[1], M. Sultan[4], Yong Qing Fu[3, ***]

[1]Department of Physics, Faculty of Science, University Teknologi Malaysia, Skudai, 81310 Johor, Malaysia
[2]Department of Physics, GPG Jehanzeb College Saidu Sharif Swat 19130, KPK, Pakistan
[3] Faculty of Engineering and Environment, Northumbria University, Newcastle upon Tyne, NE1 8ST, UK
[4] Nanoscience and Technology Department, National Centre for Physics, Islamabad, 44000 Pakistan

Abstract

In this paper, a one-step thermal evaporation approach was used for fabrication of indium bismuth sulphide thin films, and the synergetic effects of co-evaporation of two sources (indium granules and Bi_2S_3 powders) were investigated using different characterization techniques. X-ray diffraction (XRD) analysis confirmed the crystalline orthorhombic structure for the post-annealed samples. Surface roughness and crystal size of the obtained film samples were increased with increasing annealing temperatures. Analysis using X-ray photoelectron spectroscopy showed the formation of the $InBiS_3$ structure for the obtained films, which is also confirmed by the XRD results. The optical absorption coefficient value of the annealed samples was found to be in the order of 10^5 cm^{-1} in the visible region of the solar spectrum. The optical band gap energy and electrical resistivity of the fabricated samples were observed to decrease (from 2.2 to 1.3 eV, and from 0.3 to 0.01 Ω-cm, respectively) with increasing annealing temperatures (from 200 to 350°C), indicating the suitability of the prepared $InBiS_3$ thin films for solar cell applications.

Keywords: Thin films; Photovoltaics; Optical properties; XRD; Electrical properties

---

Corresponding authors: *rashidahmed@utm.my (R. Ahmed)

** nisar.ali@utm.my (Nisar Ali)

**Richard.fu@northumbria.ac.uk (Richard Y.Q. Fu)

Introduction

Recently bismuth chalcogenide based thin films have received significant attention from both scientific community and industrial counterpart. These materials generally show large absorption coefficients, good chemical stability, and band gap energies in the range from 1.2-1.7 eV, which are considered very right one for photovoltaic and thermoelectric applications [1, 2]. Some of the bismuth chalcogenides such as Bi_2S_3, BiSe, CuBiS, $CsBi_4Te_6$ also show interesting nonlinear optical characteristics, above and beyond the second harmonic effect [3, 4]. However, the key reason for their such attractive structural and optoelectronic properties is the stereochemical activity of $6s^2$ lone pair electrons of the bismuth [3]. Based on this mechanism, various micro- and nanostructures of the bismuth-containing chalcogenides were designed, synthesized, and characterized in the past decades for their potential applications in photovoltaic industries [5-8]. A number of different techniques have been used for the synthesis of these photovoltaic materials, such as sputtering, evaporation, chemical vapor deposition, molecular beam epitaxy, etc. [9]. Among these, thermal co-evaporation techniques could result in the good quality of controlled composition and compositional gradient across the films. High deposition rates, low gas entrapment, strong adhesion and minimal damage to the substrate make thermal evaporation approach the most promising for device fabrication [9, 10]. For example, a three-stage co-evaporation method was used to achieve a maximum cell efficiency of copper indium gallium sulphide (CIGS) up to about 20. 3 % at the laboratory level [11]. However, this technique has not been applied to large-scale industrial applications. Similarly, other co-evaporation techniques have been applied to the large module (1.2×0.6 m^2) at Wurih Solar, Germany [12]. In literature, there were studies for the synthesis of CuO_2 films using radical oxidation of the thermally evaporated high purity Cu films for solar cell applications [13, 14]. The treatment of N_2 plasma of the CuO_2 films resulted in an increased band gap from 1.69 to 2.42 eV. It was found that the hole density was increased from 10^{14} to 10^{15} cm^{-3} and the resistivity was decreased from 1879 to 780 Ω·cm after N_2 plasma treatment [14].

Indium chalcogenides including indium sulphide (InS), copper indium sulphide (CIS), and CIGS materials are of particular importance in the field of thin films photovoltaics [15, 16]. The environment-friendly characteristics and unique properties such as chemical stability and good transparency of the InS are suitable for photovoltaic applications. Different crystalline phases of

InS and its wide-range intermediate band gap energies ranging from 2 to 2.75 eV [17] were reported and it could be used as an alternative to the toxic CdS and a suitable material for buffer layers and window layers for photovoltaics [16, 18].

In the literature, the best efficiency value of the bismuth sulphide is reported to be 0.5% [19, 20]. A combination of InS and Bi_2S_3 could lead to a new compound with improved optoelectronic properties without having toxicity, thus is promising for usage in the solar harvesting energy devices for the next generation green energy. This is because the indium bismuth sulphide does not contain any toxic elements such as gallium or selenium, and therefore is environment-friendly [21, 22]. Moreover, development of new complex sulfides and chalcogenide halides could further improve their optoelectronic and photovoltaic applications [23].

In the present work, we investigated the $InBiS_3$ compound in the form of thin films synthesized from indium granules and Bi_2S_3 powders by one-step thermal evaporation approach and explored its potential application for the state of the art and environment-friendly energy technologies. We verified that the combination of bismuth chalcogenide and indium chalcogenide could produce a new non-toxic absorber layer for solar cell applications.

Experimental

Soda-lime glasses were used as the substrates, which were cleaned with acetone/isopropanol and deionized water in an ultrasonic bath. Indium bismuth sulphide (IBS) thin films were fabricated using a one-step dual-source thermal evaporation method by co-evaporating Bi_2S_3 powder (99.99% purity) and Indium granules (99.99% purity) from tungsten crucibles connected to a power supply. A current of ~80 A was used to evaporate Bi_2S_3 and a current of ~30 A to evaporate indium granules in a dual source evaporator for the formation of thin films. The source to substrate distance was kept at 10 cm. The as-deposited thin films were annealed in a vacuum furnace for one hour at temperatures of 200, 250, 300 and 350°C, respectively.

Structural properties of the annealed films were analyzed using X-ray diffractometry (XRD, D-8 Discover diffractometer with CuK_α radiation and a wavelength of 1.54Å). Surface morphology of the obtained thin films was characterized using a field emission scanning electron microscope (FESEM, SU8020 X-Max^N Oxford). Analysis of films using X-ray photoelectron spectroscopy (XPS) was carried out using Kratos Axis Ultra X-ray photoelectron spectrometer with Al K_α

radiation (1486.6 eV) source for elemental compositions and chemical bonding analysis. Optoelectronic properties of the obtained thin films were measured using UV-Vis spectroscopy (UV-3101PC). A 4-probe Keithley 2400 source meter was used to obtain the I-V characteristics and electrical resistance of the films.

Results and discussion:

Figure 1 shows XRD patterns of the as-deposited and annealed $InBiS_3$ thin films. The as-deposited films were found to be amorphous in nature and the film became crystallized when the annealing temperature was above 200°C. Two phases of $InBiS_3$ and $Bi_2In_4S_9$ were identified from XRD analysis when compared with JCDPS standards 00-039-0755 and 00-071-0553, respectively. For the sample annealed at 300-350°C, $In_4Bi_2S_9$ peaks disappear, and only the strong peaks of $InBiS_3$ are present as shown in Fig. 1. XRD analysis showed that the obtained annealed samples have the orthorhombic structure of $InBiS_3$. The lattice parameters (*a, b, c*) of the films were calculated from the XRD patterns shown in Fig. 1 using the following equation 1 [24]:

$$\mathrm{Sin}^2\theta = \frac{\lambda^2}{4}\left[\frac{\square^2}{a^2} + \frac{k^2}{b^2} + \frac{l^2}{c^2}\right] \quad (1)$$

The lattice parameters a = 9.927 Å, b = 3.889 Å, c = 13.222 Å were obtained from experimentally observed XRD peaks based on the film annealed at 350°C.

The average crystallite sizes of the obtained $InBiS_3$ thin films were calculated using line broadening analysis of the diffraction patterns [25]. The line broadening occurs due to small crystal sizes and microstrains generated within the films. The effects of both crystal size and strain can be separated using the Williamson-Hall method [25] in which β cos (θ) is plotted against sin (θ), where β is the full width at half maximum (FWHM) of the respective diffraction peak at 2θ. The results of Williamson-Hall plots of the annealed $InBiS_3$ thin films based on the prominent peaks of (2 0 1), (1 0 3), (1 1 1) and (2 0 6) reflections are shown in Fig. 2. Clearly, these plots can be fitted into straight lines. The value of D can be calculated from the inverse of the intercept of the line on β cos (θ) axis which gives the ratio of the crystalline grain diameter (D) to the wavelength (1.54056 Å) [25]. From the slopes of the line, the micro-strain (ε) can also be calculated.

The calculated crystallite size of the samples was observed to increase (26-64 nm) with increasing annealing temperature (250-350°C), whereas the microstrain values were in the order of 10^{-3} and found to increase with increasing annealing temperature. The increase in crystallite size is a consequence of the coalescence of small crystallites and re-orientation of crystal planes during annealing [26, 27].

Figure 3 shows the SEM images of surface morphologies of $InBiS_3$ thin films. The as-grown film has relatively smooth surface features as shown in Fig. 3 (a). As the annealing temperature is increased, the surface becomes rougher due to the coarsening of the microstructure and crystal growth. When the annealing temperature is above 250°C, in some areas, there are some larger particles which might be due to the preferred growth of some grains as shown in Figs. 3 (c) to 3 (e).

The results of chemical states for the $InBiS_3$ thin film (350°C annealed) obtained from XPS are shown in Fig. 4, indicating the existence of a key element of Bi, In and S. The peak of C1s was used as the reference to correct the peak shift due to charging effects.

The high-resolution core level spectra of the identified three elements are shown in Figs. 5 (a) to 5 (c). The magnified core level spectrum of the bismuth reveals a 4f doublet state as shown in Fig. 5 (a)**.** The peaks observed at 157.0 and 162.3 eV are related to Bi_2S_3. The binding energies of 157.0 eV and 162.3 eV are for the Bi $4f_{7/2}$ and $4f_{5/2}$ with a peak separation of 5.3 eV, and the component peaks at 163.3 and 158.0 eV are associated with Bi-O or Bi-O-S due to surface adsorption with a peak separation of 5.3 eV. The Bi-O peak is very small. The other component peaks are matched with the peak values of In doped Bi_2S_3 in the database, and their intensities are relatively low, indicating their small quantities in the sample [28, 29]. Fig. 5 (b) displays the high-resolution spectra of In $3d_{5/2}$ and $3d_{3/2}$ doublet states. The main 3d peaks were observed at binding energies of 443.5 and 451.0 eV with a peak separation of 7.8 eV, while the component

peaks at 444.2 and 451.9 eV correspond to In $3d_{5/2}$ and In $3d_{3/2}$, respectively [30]. The peaks observed at 443.5 and 451.0 eV are associated with In-S, while the other component peaks at 444.2 and 451.9 are corresponding to Bi doped In-S from the database, which causes the shifts in the energies of these peaks. The S 2p core level spectra with peak positions at 162.3, 162.9 and 163.4 eV are shown in Fig. 5 (c). The binding energies for S 2p are with the energy range between 160 and 164 eV associated with S in sulphide phases [31-33]. The ratio of the peak integrations for the In (3p), Bi (4f) and S (2s) is in the ratio 1:1:3 indicating the formation of $InBiS_3$. These results agree with that of the XRD pattern of the synthesized thin film annealed at 350 $^{\circ}$C.

Fig. 6 shows the corresponding absorption coefficient versus wavelength for as-deposited and annealed $InBiS_3$ thin films. When an electron is excited from the valence band to the conduction band at a lower wavelength, it leads to the absorption which is referred to a band-to-band transition between ionized donor and conduction band.

From the plot in Fig. 6, the absorption coefficient values of the obtained thin films increase with increasing annealing temperature, and this is more sensitive to crystal distribution on the outer layer of the thin film. The increase in the concentration of free carriers on the spectral dependency of absorbance results in an increase in the absorption of the films (Fig. 6) with a maximum value of ~ 2.5×10^4 cm^{-1}, which is comparable to the reported absorption coefficient for the established absorber material such as CdTe [34, 35]. The increase in the grain size and improvement in crystallinity after post-annealing have shifted the absorption edge towards the longer wavelength, presumably due to improved physical properties (e.g., density and fewer grain boundaries) of the thin films as a result of crystallization [36]. The fundamental absorbance spectra for the $InBiS_3$ thin films show that the absorption coefficient increases with increase in the annealing temperature [37].

The band gap was calculated from absorbance spectra using equation 2 [38].

$$(\alpha h\nu) = A(h\nu - E_g)^n \quad (2)$$

in which α is the absorption coefficient, hν is the energy of the photon, E_g is band gap while A is a constant. The plots as shown in Fig. 7 reveal that with increasing annealing temperature the band gap energy is decreased and the values are found to be in the range of 1.3 and 2.2 eV [39].

The relationship between optical energy band gaps (Fig. 8) of the films and annealing temperature can be obtained by data fitting and the equation is listed in Equation 3. Clearly the values of the optical band-gaps decrease with the increase of the annealing temperatures, similar to that reported by Larbi et al. about the tin antimony sulfide films [40].

$$E_g=1.936-6.212T-4.875T^2 \quad (3)$$

Figs. 9 and 10 show the optical transmittance (T) and reflectance (R) spectra of the fabricated $InBiS_3$ thin films, in the wavelength range from 300 to 1800 nm. The strong absorption region, i.e., the visible and near infrared region has almost no interference effect for samples annealed at 250°C and above. As-deposited and 200°C annealed samples have almost no absorbance as shown in Fig 10. However, when the annealing temperature is above 200°C, an absorption hump appears in the spectrum for the film annealed at 250°C but it does not exist in the samples for 300 and 350°C annealed samples. It is also obvious that in the transparent region, the combined values of reflection and transmission are almost equal to 1, an indication of no scattering effect [41]. The transmittance spectra as shown in Fig. 10 reveal a decreasing trend with the increasing annealing temperature which may be attributed to the increase of grain size and coarsening of crystal features due to grain growth.

The measured I-V curves for the as-deposited and post annealed $InBiS_3$ thin films are shown in Fig 11**.** Clearly, a linear relationship between current and voltage for the as deposited and annealed films can be obtained. The increase in the current is a consequence of the increment in the grain size and improvement in the crystallinity with the annealing temperature because the increase in the annealing temperature will reduce the percentage of the grain boundaries in the film and also increases the charge density, both of which lead to an increase in the electrical conductivity of the films [42, 43].

The resistivity (Fig. 12) of the samples was calculated by multiplying the thickness of the film (0.5 μm) with the resistance values of the films, which were calculated from I-V curves (Fig. 11). The decrease in resistivity of the films with the increase of annealing temperature is another indication of the improved structural and electrical characteristics of the films.

Conclusions

In summary, we have investigated thin films of the non-toxic elemental composition prepared by co-evaporating indium granules and Bi_2S_3 powders in a vacuum thermal evaporation system. From the XRD and XPS analysis, we found that the thin films annealed at 350°C have an orthorhombic phase of the $InBiS_3$ structure. Our analysis showed that with increasing annealing temperature, the grain size of the obtained films was increased, whereas the band gap value was decreased, with a value of 1.3 eV for the film annealed at 350°C. Besides its lower values of the reflectance and transmittance, and higher value of the absorption in the visible and near-infrared regions, the I-V characteristics of the thin films revealed its semiconducting nature, showing its advantages for photovoltaics. Hence, our results showed that the $InBiS_3$ can be used as an alternate material for an absorber layer in thin film solar cells.

Acknowledgements

The authors would like to thank University Teknologi Malaysia and Ministry of Education Malaysia for the financial support of this research work through project Nos Q.J130000.2526.12H46, Q.J130000.2526.16H25, Post-Doctoral Fellowship Scheme under project no: Q.J130000.21A2.02E69 and International Doctoral Fellowship, 176–BIASISWAZAH UTM IDF.

References

[1] S. Dunst, T. Rath, A. Reichmann, H.-T. Chien, B. Friedel, G. Trimmel, A comparison of copper indium sulfide-polymer nanocomposite solar cells in inverted and regular device architecture, Synthetic Metals.
[2] D. Sengupta, P. Das, B. Mondal, K. Mukherjee, Effects of doping, morphology and film-thickness of photo-anode materials for dye sensitized solar cell application – A review, Renewable and Sustainable Energy Reviews, 60 (2016) 356-376.
[3] W. Yin, D. Mei, J. Yao, P. Fu, Y. Wu, Bi 3 In 4 S 10 and Bi 14.7 In 11.3 S 38: Two new bismuth sulfides with interesting Bi–Bi bonding, Journal of Solid State Chemistry, 183 (2010) 2544-2551.

[4] N. Ali, A. Hussain, R. Ahmed, W.W. Shamsuri, Y.Q. Fu, Synthesis, and characterization of copper antimony tin sulphide thin films for solar cell applications, Applied Surface Science, 390 (2016) 393-398.
[5] M. Khadraoui, R. Miloua, N. Benramdane, A. Bouzidi, K. Sahraoui, Synthesis and characterization of (Sn 2 S 3) x (Bi 2 S 3) 1-x composite thin films for solar cell applications, Materials Chemistry and Physics, 169 (2016) 40-46.
[6] S. ten Haaf, H. Sträter, R. Brüggemann, G.H. Bauer, C. Felser, G. Jakob, Physical vapor deposition of Bi 2 S 3 as an absorber material in thin film photovoltaics, Thin Solid Films, 535 (2013) 394-397.
[7] E. Pineda, M.E. Nicho, P. Nair, H. Hu, Optoelectronic properties of chemically deposited Bi 2 S 3 thin films and the photovoltaic performance of Bi 2 S 3/P3OT solar cells, Solar Energy, 86 (2012) 1017-1022.
[8] M. Madoun, R. Baghdad, K. Chebbah, M. Bezzerrouk, L. Michez, N. Benramdane, Temperature effect on structural and optoelectronic properties of Bi 2 S 3 nanocrystalline thin films deposited by spray pyrolysis method, Materials Science in Semiconductor Processing, 16 (2013) 2084-2090.
[9] W. Kern, Thin film processes II, Academic press, 2012.
[10] L. Zang, Energy Efficiency and Renewable Energy Through Nanotechnology, Springer, 2011.
[11] P. Jackson, D. Hariskos, E. Lotter, S. Paetel, R. Wuerz, R. Menner, W. Wischmann, M. Powalla, New world record efficiency for Cu (In, Ga) Se2 thin-film solar cells beyond 20%, Progress in photovoltaics: research and applications, 19 (2011) 894-897.
[12] R. Noufi, R. Axton, C. Herrington, S. Deb, Electronic properties versus composition of thin films of CuInSe2, Applied Physics Letters, 45 (1984) 668-670.
[13] Z. Zang, A. Nakamura, J. Temmyo, Single cuprous oxide films synthesized by radical oxidation at low temperature for PV application, Optics express, 21 (2013) 11448-11456.
[14] Z. Zang, A. Nakamura, J. Temmyo, Nitrogen doping in cuprous oxide films synthesized by radical oxidation at low temperature, Materials Letters, 92 (2013) 188-191.
[15] A.A. Yadav, S. Salunke, Photoelectrochemical properties of In 2 Se 3 thin films: Effect of substrate temperature, Journal of Alloys and Compounds, 640 (2015) 534-539.
[16] N.D. Sankir, E. Aydin, E. Ugur, M. Sankir, the Non-toxic and environmentally friendly route for the preparation of copper indium sulfide based thin film solar cells, Journal of Alloys and Compounds, 640 (2015) 468-474.
[17] S. Lugo-Loredo, Y. Peña-Méndez, M. Calixto-Rodriguez, S. Messina-Fernández, A. Alvarez-Gallegos, A. Vázquez-Dimas, T. Hernández-García, Indium sulfide thin films as a window layer in chemically deposited solar cells, Thin Solid Films, 550 (2014) 110-113.
[18] M. Calixto-Rodriguez, A. Tiburcio-Silver, A. Ortiz, A. Sanchez-Juarez, Optoelectronical properties of indium sulfide thin films prepared by spray pyrolysis for photovoltaic applications, Thin Solid Films, 480–481 (2005) 133-137.
[19] M.A. Green, K. Emery, Y. Hishikawa, W. Warta, E.D. Dunlop, Solar cell efficiency tables (Version 45), Progress in photovoltaics: research and applications, 23 (2015) 1-9.
[20] H. Moreno-García, M.T.S. Nair, P.K. Nair, Chemically deposited lead sulfide and bismuth sulfide thin films and Bi2S3/PbS solar cells, Thin Solid Films, 519 (2011) 2287-2295.
[21] A. Chantiratikul, L. Borisuth, O. Chinrasri, N. Saenthaweesuk, S. Chookhampaeng, W. Thosaikham, N. Sriart, P. Chantiratikul, Evaluation of the toxicity of selenium from hydroponically produced selenium-enriched kale sprout in laying hens, Journal of Trace Elements in Medicine and Biology, 35 (2016) 116-121.
[22] C.I. Olivares, J.A. Field, M. Simonich, R.L. Tanguay, R. Sierra-Alvarez, Arsenic (III, V), indium (III), and gallium (III) toxicity to zebrafish embryos using a high-throughput multi-endpoint in vivo developmental and behavioral assay, Chemosphere, 148 (2016) 361-368.
[23] V. Krämer, Differenzthermoanalyse und kristallzüchtung im system In 2 S 3 • Bi 2 S 3, Thermochimica Acta, 15 (1976) 205-212.
[24] X.D. Xiang, I. Takeuchi, Combinatorial Materials Synthesis, Taylor & Francis, 2003.

[25] G. Williamson, W. Hall, X-ray line broadening from filed aluminum and Wolfram, Acta metallurgical, 1 (1953) 22-31.
[26] A.B. Yadav, A. Pandey, S. Jit, Effects of Annealing Temperature on the Structural, Optical, and Electrical Properties of ZnO Thin Films Grown on n-Si< 100> Substrates by the Sol–Gel Spin Coating Method, Acta Metallurgica Sinica (English Letters), 27 (2014) 682-688.
[27] N. Ali, S. Hussain, Y. Khan, N. Ahmad, M. Iqbal, S.M. Abbas, Effect of air annealing on the band gap and optical properties of SnSb 2 S 4 thin films for solar cell application, Materials Letters, 100 (2013) 148-151.
[28] S.-Y. Wang, Y.-W. Du, Preparation of nanocrystalline bismuth sulfide thin films by asynchronous-pulse ultrasonic spray pyrolysis technique, Journal of crystal growth, 236 (2002) 627-634.
[29] R. Chen, M.H. So, C.-M. Che, H. Sun, Controlled synthesis of high crystalline bismuth sulfide nanorods: using bismuth citrate as a precursor, Journal of Materials Chemistry, 15 (2005) 4540-4545.
[30] Y. Ku, P.-Y. Lin, Y.-C. Liu, Deposition of copper indium sulfide on TiO 2 nanotube arrays and its application for photocatalytic decomposition of gaseous IPA, Sustainable Environment Research, (2016).
[31] B. Yang, L. Wang, J. Han, Y. Zhou, H. Song, S. Chen, J. Zhong, L. Lv, D. Niu, J. Tang, CuSbS2 as a promising earth-abundant photovoltaic absorber material: a combined theoretical and experimental study, Chemistry of Materials, 26 (2014) 3135-3143.
[32] B. Ananthoju, F.J. Sonia, A. Kushwaha, D. Bahadur, N. Medhekar, M. Aslam, Improved structural and optical properties of Cu 2 ZnSnS 4 thin films via optimized potential in single bath electrodeposition, Electrochimica Acta, 137 (2014) 154-163.
[33] B. Pawar, S. Pawar, S. Shin, D. Choi, C. Park, S. Kolekar, J. Kim, Effect of complexing agent on the properties of electrochemically deposited Cu 2 ZnSnS 4 (CZTS) thin films, Applied Surface Science, 257 (2010) 1786-1791.
[34] J.-S. Seol, S.-Y. Lee, J.-C. Lee, H.-D. Nam, K.-H. Kim, Electrical and optical properties of Cu2ZnSnS4 thin films prepared by rf magnetron sputtering process, Solar Energy Materials and Solar Cells, 75 (2003) 155-162.
[35] S. Chander, M.S. Dhaka, Impact of thermal annealing on physical properties of vacuum evaporated polycrystalline CdTe thin films for solar cell applications, Physica E: Low-dimensional Systems and Nanostructures, 80 (2016) 62-68.
[36] F.C. Akkari, M. Kanzari, B. Rezig, Growth and properties of the CuInS 2 thin films produced by glancing angle deposition, Materials Science and Engineering: C, 28 (2008) 692-696.
[37] S. Chander, M.S. Dhaka, Optimization of physical properties of vacuum evaporated CdTe thin films with the application of thermal treatment for solar cells, Materials Science in Semiconductor Processing, 40 (2015) 708-712.
[38] M.M. Bagheri-Mohagheghi, N. Shahtahmasebi, M.R. Alinejad, A. Youssefi, M. Shokooh-Saremi, The effect of the post-annealing temperature on the nano-structure and energy band gap of SnO2 semiconducting oxide nano-particles synthesized by polymerizing–complexing sol–gel method, Physica B: Condensed Matter, 403 (2008) 2431-2437.
[39] R.B. Kale, C.D. Lokhande, Band gap shift, structural characterization and phase transformation of CdSe thin films from nanocrystalline cubic to nanorod hexagonal on air annealing, Semiconductor Science, and Technology, 20 (2005) 1.
[40] A. Larbi, H. Dahman, M. Kanzari, Effect of substrate temperature on structural and optical properties of the new high absorbent Sn 3 Sb 2 S 6 thin films, Vacuum, 110 (2014) 34-39.
[41] R. Swanepoel, Determination of the thickness and optical constants of amorphous silicon, Journal of Physics E: Scientific Instruments, 16 (1983) 1214.
[42] G. Rusu, M. Rusu, On the electrical conductivity of CdTe thin films, evaporated onto unheated substrates, Solid State Communications, 116 (2000) 363-368.

[43] N. Ali, A. Hussain, R. Ahmed, M.K. Wang, C. Zhao, B.U. Haq, Y.Q. Fu, Advances in nanostructured thin film materials for solar cell applications, Renewable and Sustainable Energy Reviews, 59 (2016) 726-737.

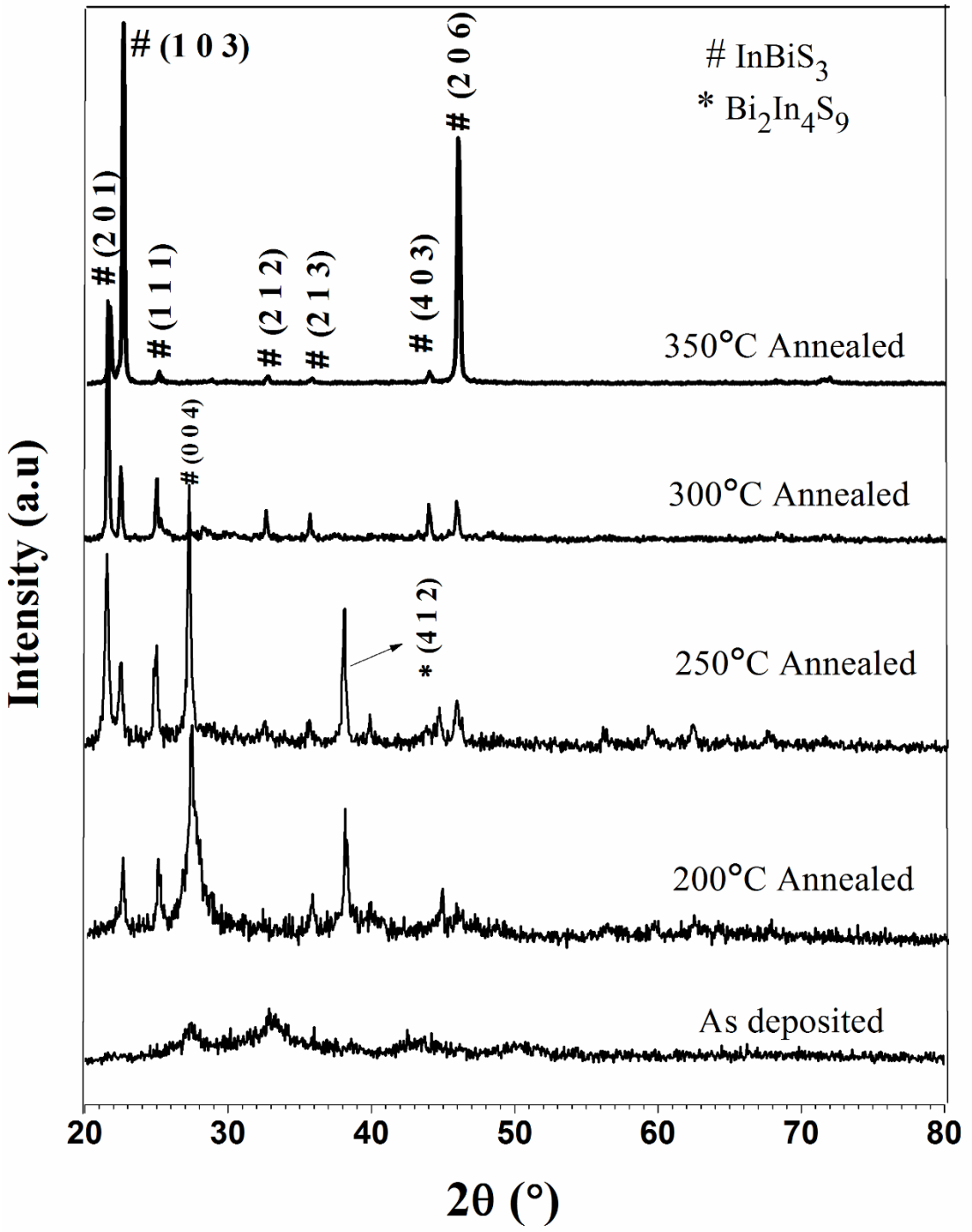

Fig 1: XRD analysis of $InBiS_3$ as deposited and annealed thin films.

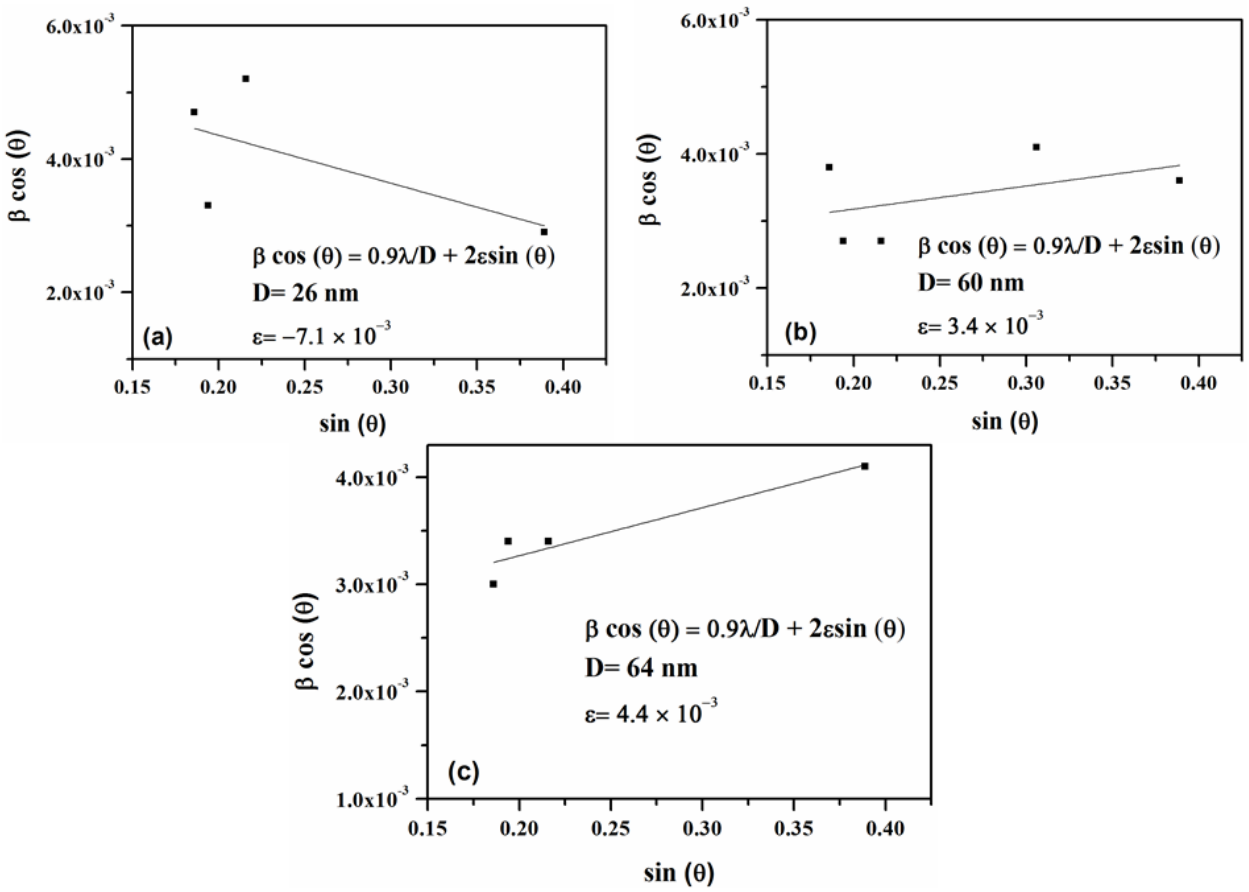

Fig 2: Plots of β cos (θ) against sin (θ) (W-H) for the obtained $InBiS_3$ thin films annealed at (a) 250˚C (b) 300˚C and (c) 350˚C

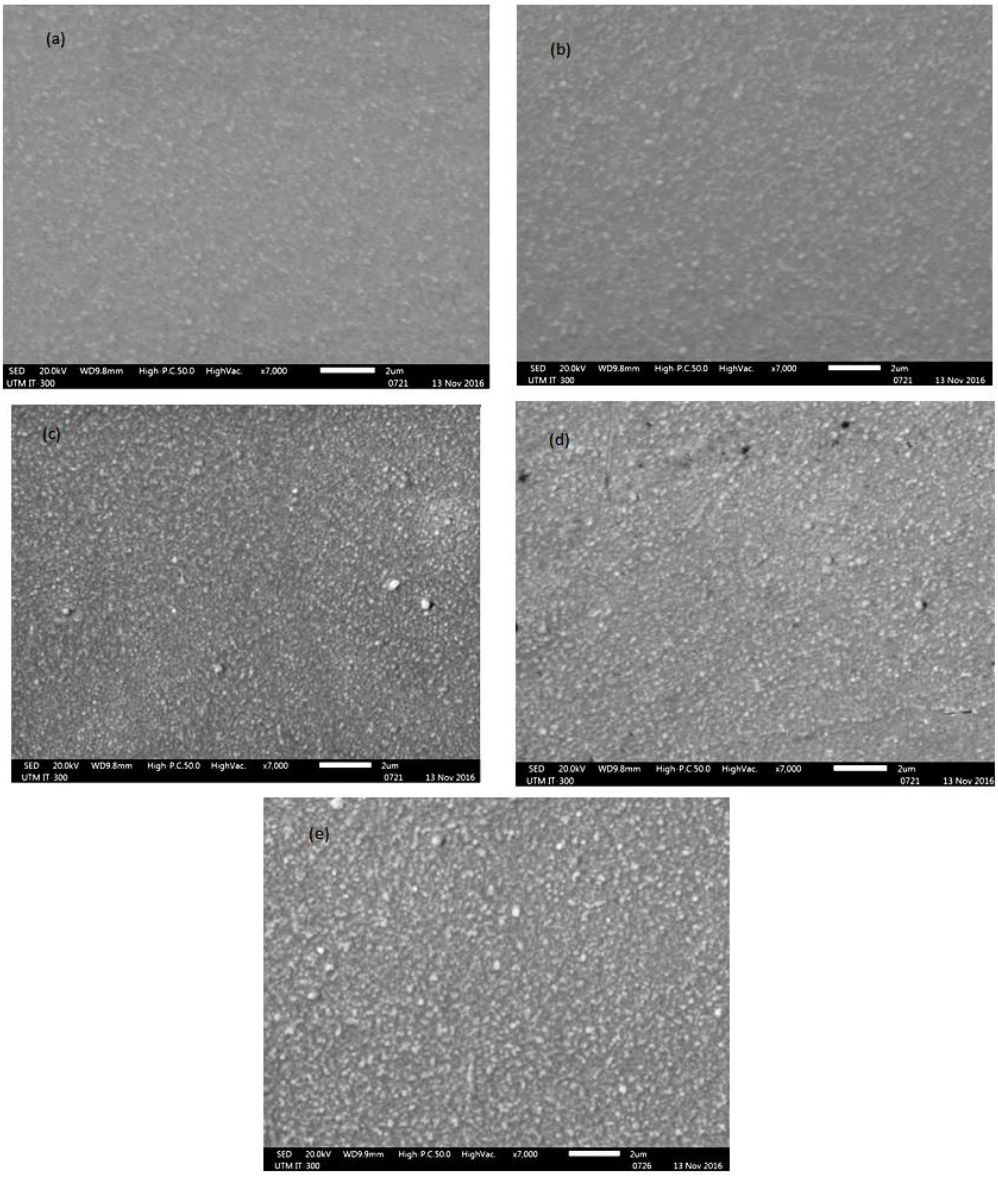

Fig 3: SEM images of $InBiS_3$ thin films (a) as-deposited (b) 200˚C annealed (c) 250˚C annealed (d) 300˚C annealed (e) 350˚C annealed sample

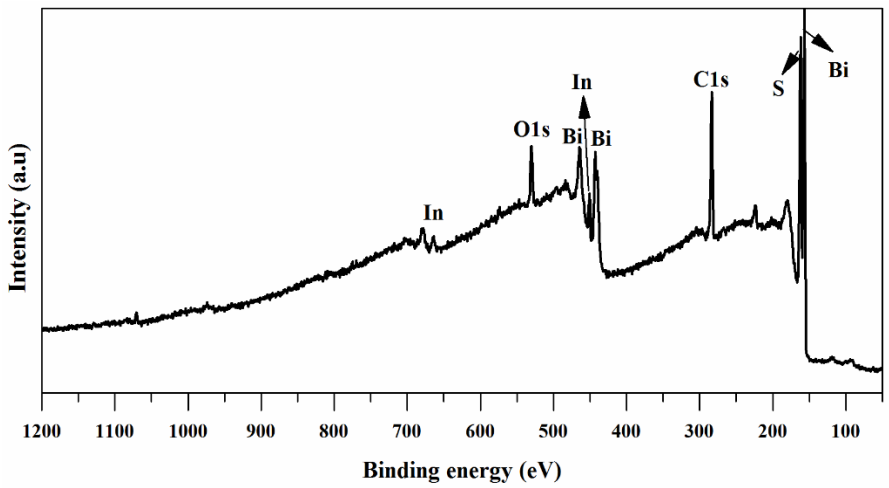

Fig. 4: XPS survey spectra of $InBiS_3$ thin film annealed at 350°C in vacuum.

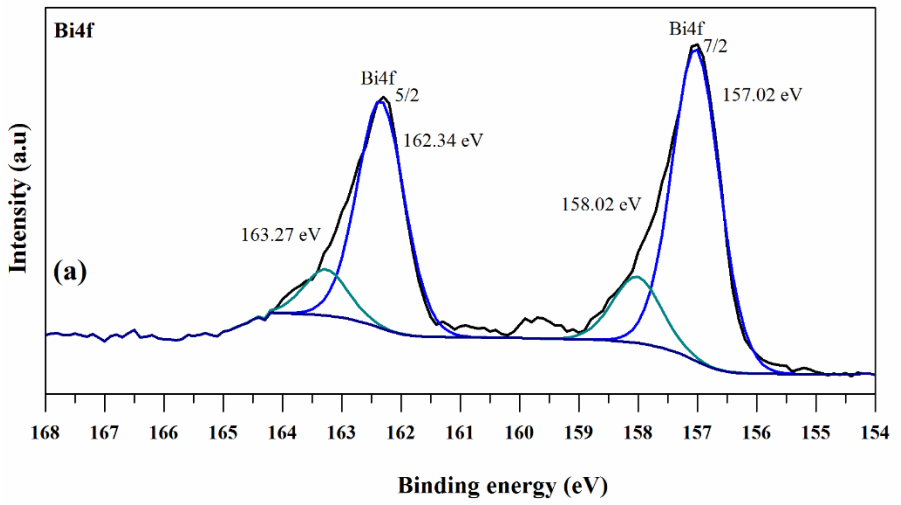
Bi4f
Bi4f 5/2
162.34 eV
163.27 eV
Bi4f 7/2
157.02 eV
158.02 eV
(a)
Intensity (a.u)
168 167 166 165 164 163 162 161 160 159 158 157 156 155 154
Binding energy (eV)

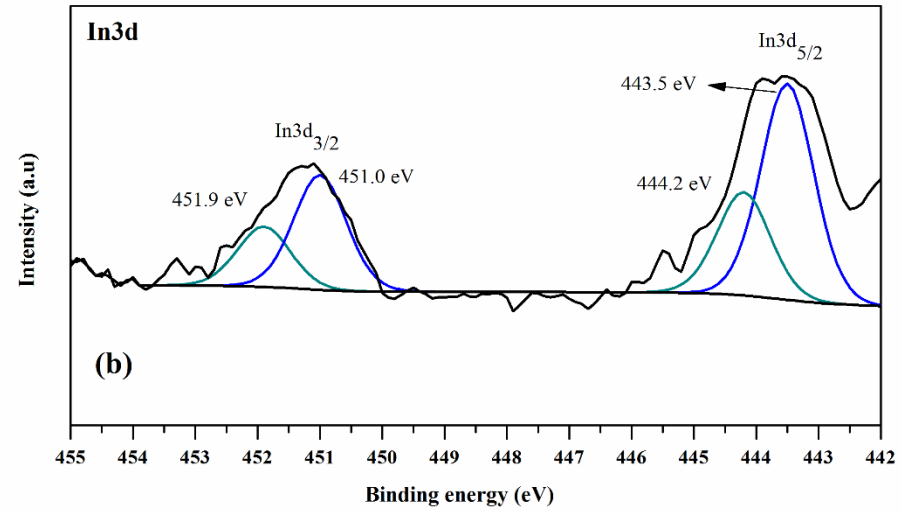
In3d
In3d 5/2
443.5 eV
In3d 3/2
451.0 eV
451.9 eV
444.2 eV
(b)
Intensity (a.u)
455 454 453 452 451 450 449 448 447 446 445 444 443 442
Binding energy (eV)

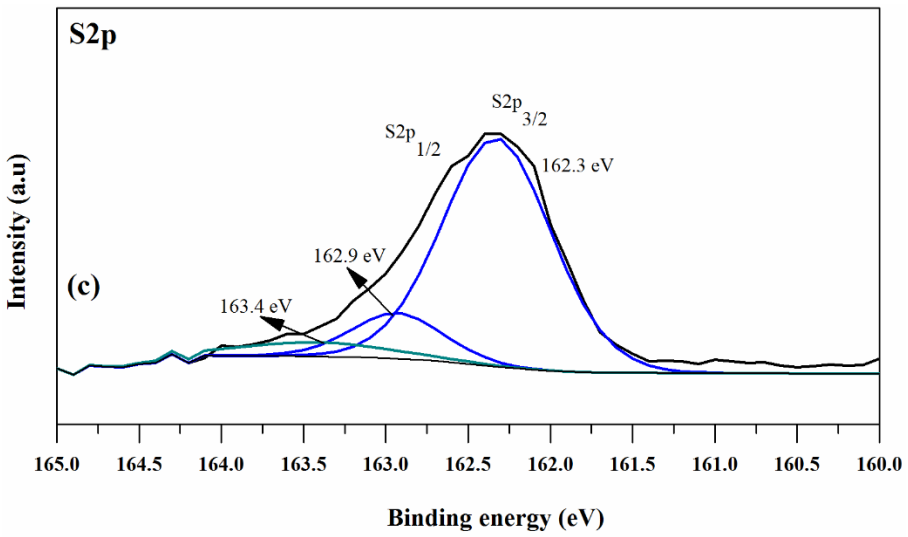

Fig 5: High-resolution spectra of (a) Bi 4f core level (b) In 3d core-level and (c) S 2p core level of $InBiS_3$ thin film annealed at 350^{o}C in a vacuum.

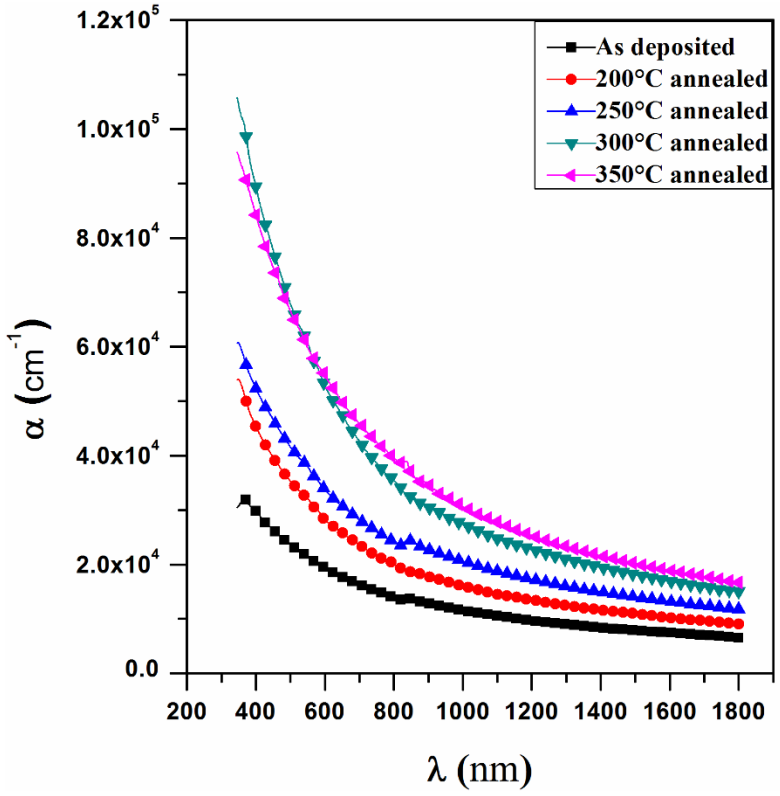

Fig 6: Absorption coefficient of the as-deposited and annealed $InBiS_3$ samples.

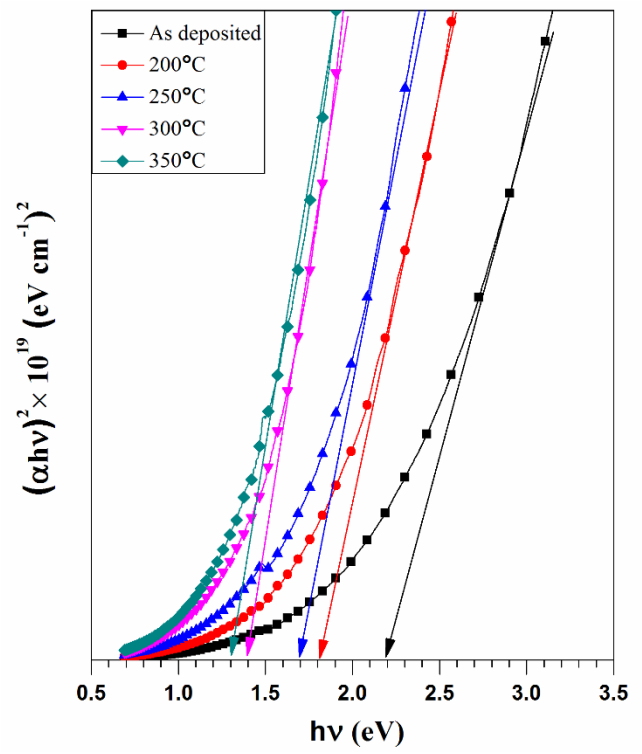

Fig 7: Band gap measurements from absorption spectra for the as-deposited and annealed samples.

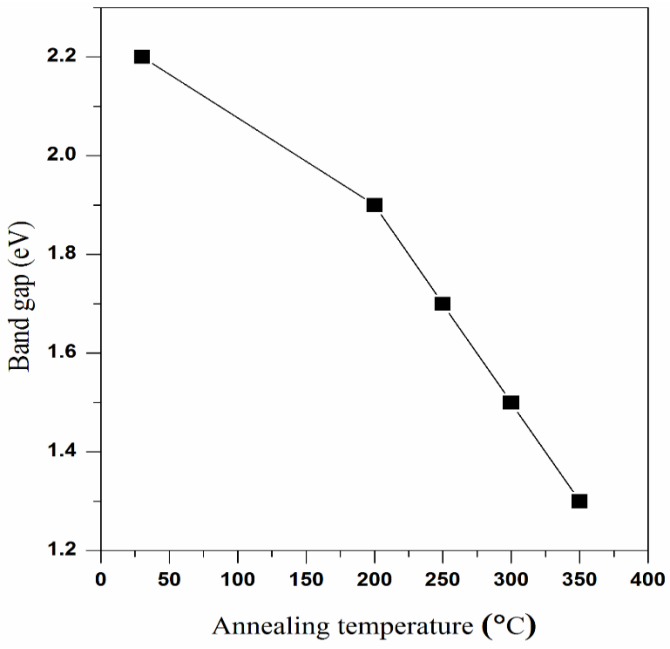

Fig 8: Band gap values as a function of annealing temperature.

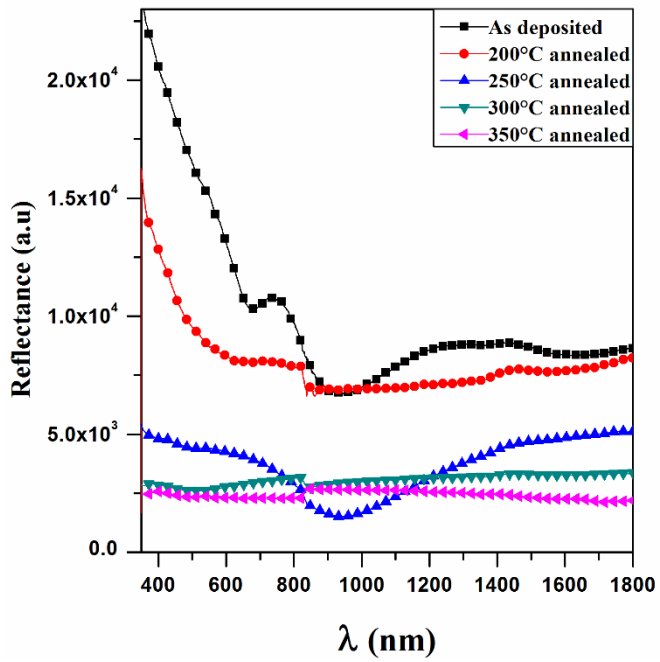

Fig 9: Reflectance spectra of the as-deposited and annealed $InBiS_3$ thin film samples.

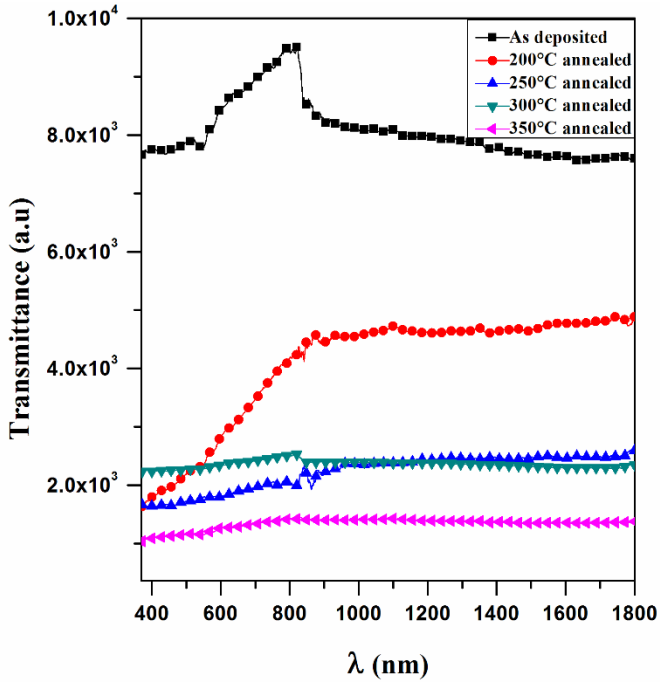

Fig 10: Transmittance spectra of the as-deposited and annealed $InBiS_3$ thin films.

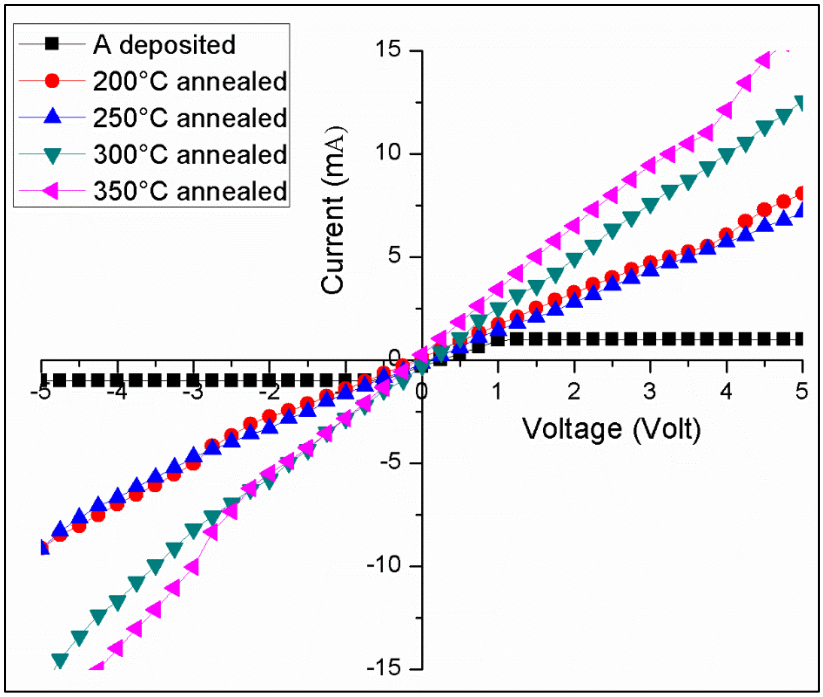

Fig 11: The transverse current–voltage characteristics of as-deposited and annealed $InBiS_3$ thin films.

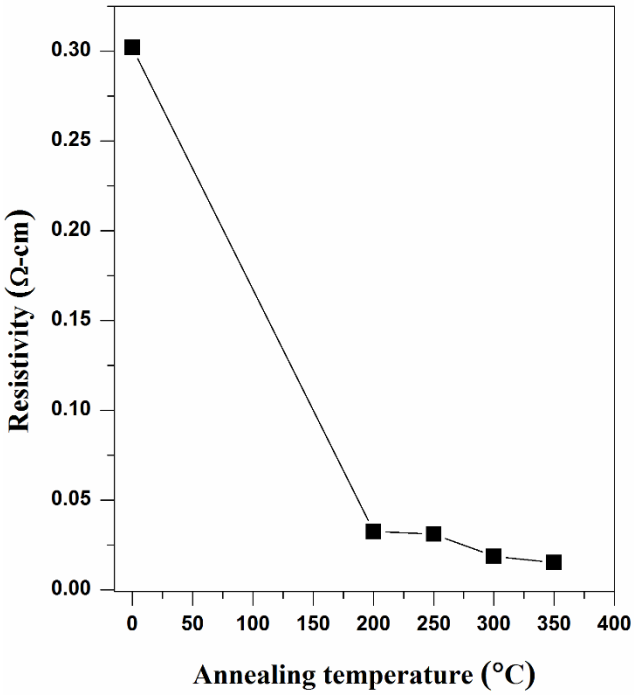

Fig 12: Variation of resistivity with annealing temperature.